Volume 11
Number 15
21 April 2023
Pages 3265–3474

Journal of Materials Chemistry B

Materials for biology and medicine

rsc.li/materials-b

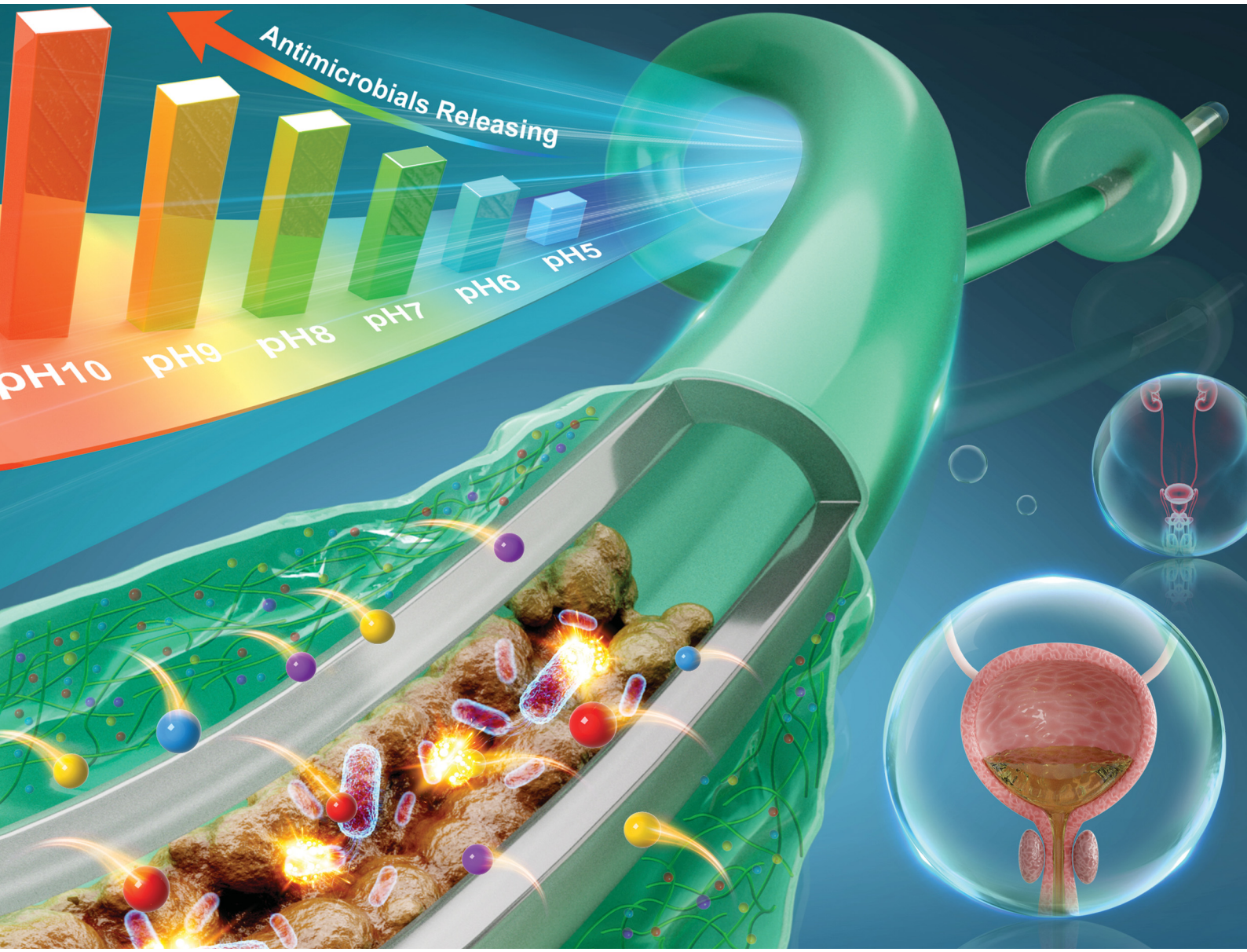

ISSN 2050-750X

ROYAL SOCIETY OF CHEMISTRY

PAPER

Mi Ouyang, Rong Wang *et al.*
Multifunctional hydrogel coatings with high antimicrobial loading efficiency and pH-responsive properties for urinary catheter applications

10 YEARS ANNIVERSARY

Journal of Materials Chemistry B

ROYAL SOCIETY OF CHEMISTRY

PAPER

View Article Online
View Journal | View Issue

Cite this: J. Mater. Chem. B, 2023, 11, 3373

Multifunctional hydrogel coatings with high antimicrobial loading efficiency and pH-responsive properties for urinary catheter applications†

Jiru Miao,[ab] Xiang Wu,[bc] Yue Fang,[b] Mingzhu Zeng,[b] Zhimao Huang,[b] Mi Ouyang *[a] and Rong Wang *[bd]

Catheter-associated urinary tract infections are one of the most common hospital-acquired infections. Encrustation formation results from infection of urease-producing bacteria and further complicates the situation. A typical sign of the initial onset of encrustation formation is the alkalization of the urine (pH up to 9–10). However, effective antibacterial strategies with high antimicrobial loading efficiency and pH-responsiveness of antimicrobial release are still lacking. In this study, we developed a poly(sulfobetaine methacrylate)-tannic acid (polySBMA-TA) hydrogel coating, which served as a universal, efficient, and responsive carrier for antimicrobials on urinary catheters. Common antimicrobials, including poly(vinylpyrrolidone)-iodine, copper ions, and nitrofurazone were loaded into the polySBMA-TA coating in high efficiency (several fold higher than that of the polySBMA coating), *via* the formation of multiple non-covalent interactions between the antimicrobials and hydrogel coating. The hydrogel coatings maintained good antibacterial properties under neutral conditions. More importantly, the pH-responsive release of antibacterial agents under alkaline conditions further enhanced the antibacterial activity of the coatings, which was advantageous for killing the urease-producing bacteria and preventing encrustation. *In vitro* and *in vivo* tests confirmed that the hydrogel coating has good biocompatibility, and could effectively inhibit bacterial colonization and encrustation formation. This study offers new opportunities for the utilization of a simple and universal antimicrobial-loaded hydrogel coating with smart pH-responsive properties to combat bacterial colonization and encrustation formation in urinary catheters.

Received 25th January 2023,
Accepted 17th March 2023

DOI: 10.1039/d3tb00148b

rsc.li/materials-b

1. Introduction

Urinary catheters have become one of the most commonly used medical devices in hospitals since the model was designed in the 1930s. However, catheter-associated urinary tract infections (CAUTIs) account for approximately 9% of hospital-acquired infections (HAIs) in the United States,[1] making it one of the major HAIs. The surface of a urinary catheter provides an ideal site for adhesion, colonization, and proliferation of uropathogens like *Escherichia coli* (*E. coli*) and *Proteus mirabilis* (*P. mirabilis*).[2] Bacterial biofilm formed on the catheter surface is difficult to fully eradicate, leaving removal of the infected catheter the only choice. More importantly, some bacteria like *P. mirabilis* can generate urease, which breaks down urea into ammonia, resulting in alkalization of the urine.[3] In the alkalized condition, calcium and magnesium phosphates deposit onto the catheter surface, forming encrustations that block the catheter lumen rapidly within 1–2 days from the onset of infection. The consequence of encrustation is catastrophic since retention and/or reflux of the infected urine increase the risk of upstream infections, sepsis, and even death. It was reported that up to 50% of patients with long-term catheterization suffer from encrustation.[3] Therefore, the development of effective strategies to inhibit bacterial colonization and bacteria-inducing encrustation in urinary catheters is highly desired.[4,5]

[a] College of Chemical Engineering, Zhejiang University of Technology, Hangzhou, 310014, P. R. China. E-mail: ouyang@zjut.edu.cn
[b] Zhejiang International Scientific and Technological Cooperative Base of Biomedical Materials and Technology, Zhejiang Engineering Research Center for Biomedical Materials, Cixi Institute of Biomedical Engineering, Ningbo Institute of Materials Technology and Engineering, Chinese Academy of Sciences, Ningbo, 315300, P. R. China. E-mail: rong.wang@nimte.ac.cn
[c] Department of Hepatobiliary and Pancreatic Surgery, Affiliated Li Huili Hospital, Ningbo University School of Medicine, Ningbo, 315000, China
[d] University of Chinese Academy of Sciences, Beijing, 101408, P. R. China
† Electronic supplementary information (ESI) available. See DOI: https://doi.org/10.1039/d3tb00148b

Numerous efforts have been made, through chemical immobilization or physical absorption of antimicrobials on the catheter surface,[6–10] and impregnation of antimicrobials in swollen catheter materials,[11,12] to inhibit bacterial infection and encrustation. However, the current strategies for the development of antimicrobial urinary catheters suffer from some limitations. First, the coating process is complex, and it may be incompatible with the catheter material due to the use of harsh solvents.[13,14] Second, the concentration and types of antimicrobial agents loaded or immobilized are limited, restraining the broad antibacterial spectrum of the coating, and increasing the concern of potential antibiotic resistance.[5,15] Lastly, but most importantly, conventional coatings could not detect the urinary conditions to predict or respond to the onset of encrustation, while the release of an effective concentration of antimicrobials to kill the urease-producing bacteria is of paramount importance to stop the progress of encrustation formation.[16]

Ideally, an effective antimicrobial catheter surface should maintain prolonged release of antimicrobials, to reduce the risk of infection during its use, and offer fast release of a sufficiently high concentration of antimicrobials, to enhance its antibacterial efficacy as early as possible if a urease-positive bacterial infection is detected and encrustation is predicted. As mentioned above, encrustation occurs because of urine alkalization. Thus, the change in the urine pH is a reliable predictor of encrustation and catheter blockage. Indeed, several pH-responsive sensors have been developed and integrated into an urinary catheter system, to obtain an ''early warning'' of catheter blockage.[17–19] More recently, novel coatings to release antimicrobials or bacteriophage in a pH-responsive manner to inhibit encrustation formation have been reported.[20,21] For instance, Milo *et al.* reported a dual-layer system with a lower layer containing bacteriophage capped by an upper pH-responsive polymer layer.[20] The coating was stable in conditions without infection, or in the presence of urease-negative bacteria, but a burst release of bacteriophage occurred in response to infection with urease-positive bacteria. Zhou *et al.* reported a theranostic multilayer coating with the capability of early visual warning of catheter blockage and antibacterial efficacy.[21] These studies show a novel way of utilizing smart antimicrobial coatings with pH responsiveness against encrustation formation.

In this study, we report a pH-responsive hydrogel coating with a high loading efficiency of common antimicrobial agents for combating bacterial colonization and encrustation formation. A poly-zwitterionic hydrogel coating was first prepared on the catheter surface by free radical polymerization. Natural polyphenol tannic acid (TA) was incorporated in the zwitterionic polysulfobetaine methacrylate (polySBMA) hydrogel layer *via* multiple non-covalent interactions including hydrogen bonding and electrostatic interactions. Different commonly used antimicrobial agents, *i.e.* poly(vinylpyrrolidone)-iodine (PVP-I), copper ions, and nitrofurazone, were loaded into the polySBMA-TA coating *via* a simple and green impregnation process. The loading efficiency and pH-responsive release profile of the hydrogel coating were investigated. The *in vitro* antibacterial and anti-encrustation properties, cytotoxicity, and *in vivo* performance of the antimicrobial-loaded hydrogel coating were evaluated.

2. Materials and methods

2.1 Materials

[2-(Methacryloyloxy)ethyl]dimethyl-(3-sulfopropyl)ammonium hydroxide (sulfobetaine methacrylate, SBMA, 97%), tannic acid (TA, 95%) and ammonium persulfate (APS, 98%) were purchased from Aladdin Chemistry (Shanghai, China). Copper(II) sulfate was obtained from Sinopharm (Shanghai, China). Poly(ethylene glycol) dimethacrylate (Mn 550 Da) was purchased from Sigma-Aldrich (Shanghai, China). Benzoyl peroxide was purchased from Energy Chemical (Shanghai, China). Nitrofurazone was purchased from J & K Scientific (Beijing, China). Poly(vinylpyrrolidone)-iodine (PVP-I) was purchased from Hubei Ketian Pharmaceutical (Hubei, China). Artificial urine (Catalogue No. A6660), Cell Counting Kit-8 (CCK-8), Calcein/PI Cell Viability/Cytotoxicity Assay Kit, and hematoxylin and eosin (H & E) staining kit (Catalogue No. G1120) were purchased from Solarbio Life Sciences (Beijing, China). *Escherichia coli* (*E. coli*) ATCC 25922 was purchased from American Type Culture Collection, and *Proteus mirabilis* (*P. mirabilis*) CMCC 49005 was purchased from Shanghai Bioresource Collection Center. NIH/3T3 fibroblast cells (Catalogue No. SCSP-515) were obtained from the National Collection of Authenticated Cell Cultures, Chinese Academy of Sciences. SYL-GARD™ 184 Silicone Elastomer Kit was obtained from Dow Chemical (Michigan, United States), and used to prepare a flat polydimethylsiloxane (PDMS) sheet (0.1 cm thickness) following the manufacturer's instruction. Silicone Foley catheters (8 Fr) were purchased from Well Lead Medical (Guangzhou, China).

2.2 Preparation of hydrogel coating

Flat PDMS sheets were cut into sizes of 1 cm × 3 cm, cleaned with ethanol, and subjected to glow discharge treatment at a current of 15 mA for 3 min (Glow Discharge Cleaning System, easiGlow 91000, PELCO, United States). The PDMS sheets were then soaked in a benzoyl peroxide solution (10 wt% in acetone) for 5 min, followed by washing with isopropanol, and drying in nitrogen. A pre-gel solution containing 22.3 g of SBMA, 90 mg of poly(ethylene glycol) dimethacrylate, 23 mg of ammonium persulfate, and 20 mL of deionized water was prepared, and 3.7 g of TA (8 wt% of the total weight of the solution) was added. The pre-gel solution was degassed using nitrogen bubbling for 30 min. The PDMS sheet was immersed in the solution, and it was placed in a water bath at 80 °C for 90 min to thermally initiate the polymerization. The PDMS sheet with hydrogel coating formed on its surface was collected, and washed using deionized water. The PDMS sheets with hydrogel coatings prepared from solution with and without 8 wt% of TA were denoted as PT8 and PT0, respectively. After that, the

PT8-coated substrate was immersed in 10 mL of physiological saline solution containing 10 mg mL^{-1} PVP-I, 11.25 mg mL^{-1} copper sulfate, or 0.2 mg mL^{-1} nitrofurazone (common concentrations used in the clinic for antibacterial purposes) at 37 °C for 24 h. The antimicrobial-loaded coatings were named PT8-I, PT8-Cu and PT8-NFZ, respectively. PDMS and PT0 substrates were treated with the antimicrobial agent solution in the same procedure for comparison. The concentration of iodine and copper in the solution before and after the coating process was determined by inductively coupled plasma optical emission spectrometry (ICP-OES, ARCOS, SPECTRO, Germany). The concentration of nitrofurazone was determined by measuring the absorbance of the solution at 375 nm using a UV-Vis spectrophotometer (Cary 300, Agilent, United States). The loading content of the antimicrobial agents in the coating was calculated by subtracting the remaining content of antimicrobial agents in the solution from the total content. Silicone Foley catheters were coated in the same procedure for *in vivo* implantation experiments.

2.3 Coating characterization

The cross-section of PDMS samples was obtained after fracture in liquid nitrogen, and observed using scanning electron microscopy (SEM, regulus 8230, Hitachi, Japan). The coating thickness was calculated using ImageJ software (Version 1.52a). The surface hydrophilicity of the sample was measured using a contact angle goniometer (DSA25E, KRUSS, Germany). Elements on pristine and modified PDMS surfaces were characterized using X-ray photoelectron spectroscopy (XPS, Axis Ultra DLD, Kratos, United Kingdom).

The PDMS substrate was cut into dumbbell shapes with 2 cm in narrow parallel width and 3.5 cm in length, and the tensile properties of the substrate were tested on a universal testing machine (CMT-1104, SUST, China) at a crosshead speed of 20 mm min^{-1}. For the friction test, hydrogel coating on the PDMS ball (diameter of 6 mm) was prepared using the same procedure as described above. The coefficient of friction (COF) of PDMS ball on the glass surface in artificial urine was measured in a tribometer (UMT TriboLab, BRUKER, Germany) in reciprocating mode, with a fixed load of 5 N, a sliding distance of 10 mm for each cycle, and a sliding speed of 5 mm s^{-1} for 300 cycles.

2.4 Release profile of the antimicrobial agent

Substrates with a size of 1 cm × 3 cm × 0.1 cm were incubated in 10 mL of phosphate buffered saline (PBS) solution at pH of 7 or 10 at 37 °C. Every 24 h, the solution was replaced with fresh one. The collected solution was subjected to ICP-OES measurement for iodine and copper quantification, and UV-Vis spectrophotometer for nitrofurazone quantification. The cumulative release of the antimicrobial agent was calculated by summing up the daily release amount.

For determination of the bactericidal property, the substrate was treated with bacterial suspension with different pH values. Briefly, overnight *P. mirabilis* culture was resuspended in PBS (pH = 7 or 10) at a concentration of 10^8 CFU per mL. Samples of 1 cm × 1 cm × 0.1 cm were placed in a centrifugal tube, immersed in 2 mL of bacterial suspension, and incubated at 100 rpm and 37 °C for 24 h. The number of viable bacteria in the solution was then counted using the spread plate method.

2.5 Antibacterial assay

For the bacterial adhesion test, overnight bacterial culture was collected and resuspended in PBS at a concentration of 10^8 CFU per mL. Samples of 1 cm × 1 cm × 0.1 cm were placed in a 24 well plate, covered with 1 mL of the bacterial suspension, and incubated statically at 37 °C. After 4 h, the bacterial suspension was aspirated, and the samples were washed with PBS to remove any unadhered bacterial cells. For qualitative analysis, pristine and modified PDMS sheets were slid onto an agar plate. The adherent bacteria on the PDMS surface were fixed in 3% glutaraldehyde, dehydrated with gradient ethanol, and observed using SEM. For cell quantification, the adherent bacteria were removed by sonication for 10 min, serially diluted, and counted using the spread plate method.

For the biofilm formation test, overnight bacterial culture was diluted in fresh culture medium to a concentration of 10^5 CFU per mL. One mL of the bacterial suspension was added to each well of a 24 well plate containing a 1 cm × 1 cm × 0.1 cm sized sample. The culture medium was changed every 24 h, and the bacteria was cultured at 37 °C for up to 10 days. For qualitative analysis, pristine and modified PDMS sheets with adherent bacteria were slid onto an agar plate. The biofilm formed on the substrate surface was observed using SEM. The bacteria on the substrate surface were also counted using the spread plate method.

2.6 Coating stability test

Hydrogel coatings on PDMS balls (diameter of 6 mm) were prepared with the same procedure as described above. PDMS balls were fixed in a tribometer and rubbed on the glass surface in artificial urine for a total travelling distance of 300 cm. The surface of the PDMS balls after the friction test was subjected to the bacterial test and contact angle measurement as described above.

2.7 *In vitro* encrustation formation

Samples of 1 cm × 1 cm × 0.1 cm were placed in 2 mL of fresh artificial urine containing 10^8 CFU per mL of *P. mirabilis*, and incubated at 37 °C with 100 rpm shaking. Every 24 h, the pH of the artificial urine was recorded, and the medium was replaced with freshly prepared artificial urine containing 10^8 CFU per mL of *P. mirabilis*. Encrustation formation on the substrate surface was observed using SEM. On days 1, 3, and 7, the substrate was collected, and the formed encrustation on the surface was digested using concentrated nitric acid, and quantified using ICP-OES.

2.8 Cytotoxicity assay

An *in vitro* cytotoxicity assay was conducted according to international standard ISO 10993-5. A 1 cm × 3 cm × 0.1 cm sample was placed in 5.44 mL of Dulbecco's Modified Eagle Medium (DMEM, supplemented with 10% fetal bovine serum, 10^5 U L^{-1} penicillin and 100 mg L^{-1} streptomycin, surface area to volume

ratio of 1.25 cm^2 mL^{-1}) at 37 °C with 5% CO_2 for 24 h. Meanwhile, NIH/3T3 fibroblasts were seeded in a 96 well plate at a concentration of 10^4 cells per well. After incubation at 37 °C for 24 h, the cell culture medium was replaced with 100 μL of the sample extract, and the cells were incubated for another 24 h. In the control group, the culture medium was replaced with 100 μL of fresh DMEM. The viability of the cells in each well was determined using CCK-8 assay according to the manufacturer's protocol. For microscopy observation, 100 μL of cell suspension at a concentration of 10^5 cells mL^{-1} was seeded in a confocal culture dish, and incubated at 37 °C. After 24 h, the medium was replaced by the same amount of extract as described above. The cells were cultured for another 24 h, followed by staining with Calcein/PI Cell Viability/Cytotoxicity Assay Kit, and then observed using confocal laser scanning microscopy (CLSM, TCS SP8, Leica, Germany).

2.9 *In vivo* implantation evaluation

The animal experiment was conducted according to the national guidelines with the approval by the Institutional Animal Ethics Committee of Ningbo University. The *in vivo* performance of the coating was evaluated by implanting the catheter in male New Zealand rabbits (2–3 kg) following our previous work.[10] An ethylene oxide-sterilized silicone catheter (8 Fr, pristine or PT8-I coated) was inserted into the bladder of the rabbit through the urethra. Three mL of sterile saline was injected to inflate the balloon, and the external part of the catheter was sutured to the rabbit's abdomen to fix the catheter. The health condition of the rabbit was monitored daily. Blood and urine samples were collected from the rabbits at the determined time point for a routine test. After 7 days, the animals were sacrificed, and the bladder, urethra, kidney, and catheter were collected. The bacterial content in the urine was determined by plate counting. The interested tissues were fixed in 10% formalin, stained with H & E, and observed using an optical microscope (DFC450 C, Leica, Germany). Encrustation formation on the catheter surface was analyzed by SEM and Energy-Dispersive X-ray Spectroscopy (EDS). For quantification, the encrustation on the catheter surface was dissolved by nitric acid digestion, and the content of calcium and magnesium was determined by ICP-OES.

2.10 Statistical analysis

All data were presented as the mean ± standard deviation. Analysis of data was performed with IBM SPSS Statistics 26 (IBM Corporation, United States). The difference among different groups was compared with one-way ANOVA followed by a Tukey's test, and statistically significant differences were marked with $*p < 0.05$, $**p < 0.01$, $***p < 0.001$. All tests were performed at least in triplicate.

3. Results and discussion

3.1 Preparation and characterization of hydrogel coatings

Poly-zwitterionic hydrogel coatings were constructed on the PDMS surface using the reported ''interfacial interpenetration strategy'' (Scheme 1a).[22] The PDMS surface was first activated by glow discharge, treated with hydrophobic initiator dibenzoyl peroxide, and then grafted with polySBMA coating *via* free radical polymerization. TA was added to the pre-gel solution, and formed a hybrid polySBMA-TA hydrogel coating due to the formation of hydrogen bonding and electrostatic interactions between zwitterionic groups and TA, as reported in our previous work.[23] Finally, different types of commonly used antimicrobial agents (*e.g.* PVP-I, Cu, nitrofurazone) were loaded in the hydrogel coating using a one-step impregnation method. The zwitterionic groups of polySBMA and phenolic hydroxyl groups of TA could form electrostatic interactions, hydrogen bonding, or coordinate bonding with the various antimicrobial molecules (Scheme 1b), and thus the polySBMA-TA hydrogel coating (PT8) served as a universal platform for antimicrobial loading.

SEM observation confirms the formation of a sub-micron hydrogel coating on the PDMS surface (Fig. 1a and b). PolySBMA formed a coating (*i.e.* PT0) with a thickness of ~0.44 μm. With the addition of TA, the thickness of the obtained coating (PT-8) increased to 0.62 μm. Loading of PVP-I and nitrofurazone resulted in a thicker coating (0.80 μm and 0.95 μm, respectively), probably due to swelling of the hydrogel layer during impregnation. The thickness of PT8-Cu was 0.65 μm, which was comparable to that of PT8, probably due to the coordination of Cu with TA forming a dense structure in the hydrogel. Contact angle measurement showed a significant decrease of surface hydrophobicity from 118° to 43° after PT0 coating, and the addition of TA in the coating further decreased the water contact angle to about 28° (Fig. 1c). Loading of PVP-I, Cu, and nitrofurazone did not result in a significant change in the surface hydrophilicity. The chemical composition of the PDMS surface before and after modification was analyzed by XPS (Fig. 1d–f and Table S1, ESI†). The C–S peak at ~287.0 eV in the C 1s core-level spectrum of PT0 was attributed to the $-SO_3^-$ group of polySBMA (Fig. 1d). The content of the C–O peak in the spectrum of PT8 increased due to the addition of TA (Table S1, ESI†), indicating that the hydrogel coating was formed on PDMS. The C═O, C–N and C–O peaks of PT8-NFZ increased as compared to that on the PT8 coating, indicating the successful loading of nitrofurazone in the coating. The I_2 and I_3^- peaks at ~630.0 eV and ~615.5 eV (Fig. 1e), and Cu $2p_{1/2}$ and Cu $2p_{3/2}$ peaks at ~954.7 eV and ~934.6 eV (Fig. 1f) could be observed on the PT8-I and PT8-Cu surfaces, respectively, confirming the successful loading of PVP-I and Cu in the coating. The surface characterization results confirmed the successful construction of hydrogel coatings of PT0 and PT8 on PDMS, and common antimicrobial agents can be loaded in the hydrogel coating in a convenient one-step impregnation method.

The tensile test showed there was no significant difference in fracture strength between the pristine PDMS and modified PDMS, and no stress yielding of the substrate was observed (Fig. S1, ESI†), indicating that the coating process did not impair the mechanical properties of PDMS. A lubricating surface is beneficial for urinary catheter application by reducing pain and tissue damage to the patient during insertion. The COFs

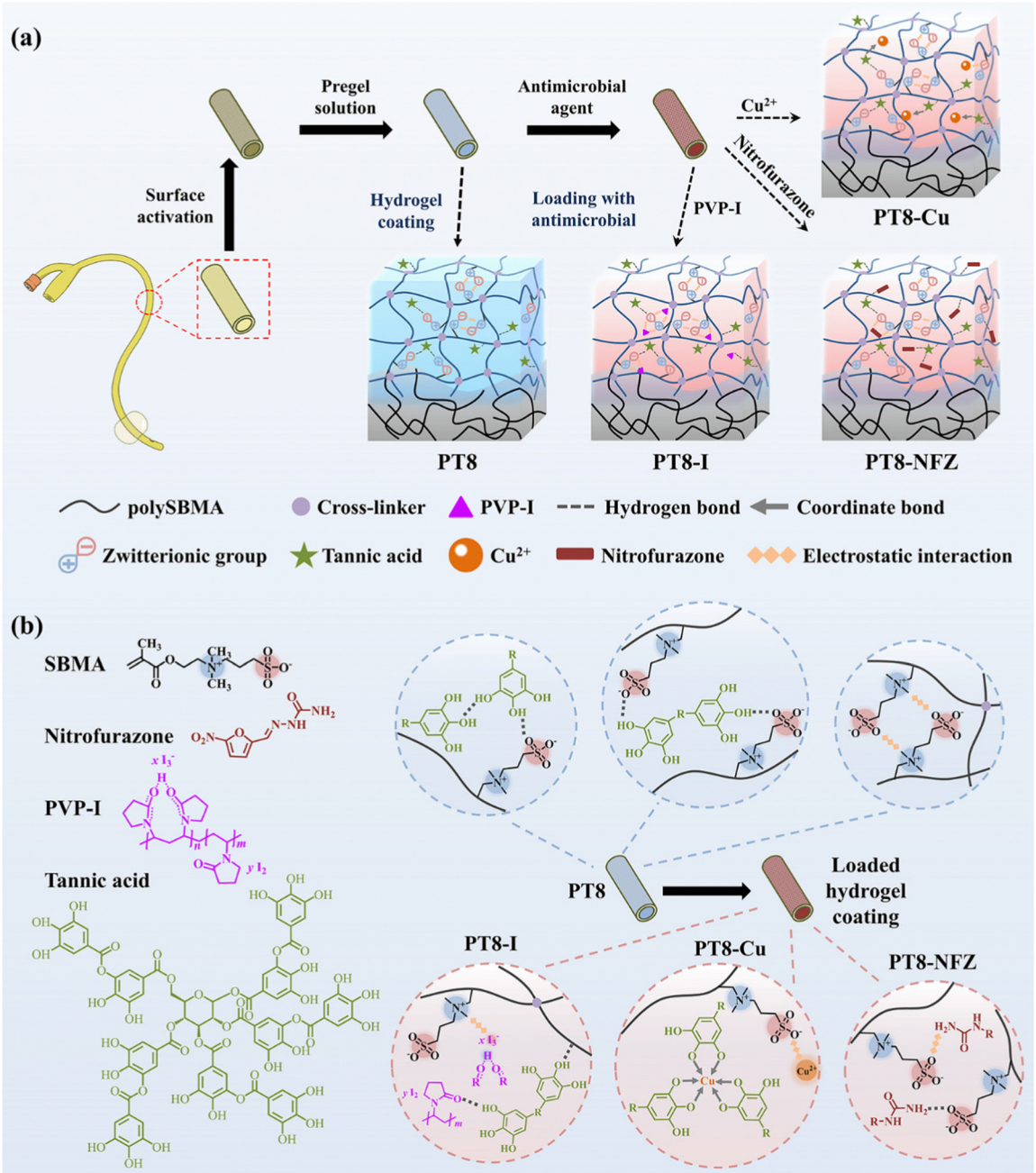

Scheme 1 Schematic diagram illustrating (a) the preparation process of a multifunctional hydrogel coating on a urinary catheter surface, and (b) the structure of PT8 hydrogel coating, and antimicrobial-loaded hydrogel coating (*i.e.* PT8-I, PT8-Cu, and PT8-NFZ).

of pristine and modified PDMS surfaces on glass in artificial urine were measured using a tribometer (Fig. S2, ESI†). The friction behavior of the pristine PDMS surface was unstable as the COF decreased as a function of sliding time. This is probably because the PDMS surface was gradually hydrated in artificial urine during the test. The friction of hydrogel coating was quite stable during the measurement (10 min, with a total travelling distance of 300 cm), as the coating was hydrophilic and hydrated immediately. The COF decreased significantly from 0.21 of pristine PDMS to 0.10 of PT0, and further decreased to 0.06 of PT8. Loading of antimicrobial agents in the hydrogel coating did not significantly change the surface frictional properties.

3.2 Loading efficiency of antimicrobials in hydrogel coating

Various types of antimicrobials, such as antimicrobial peptides,[24] silver[25] and chlorhexidine,[26] have been loaded on the catheter surface for antibacterial purposes. A high loading content of antimicrobials in the catheter is necessary for maintenance of the effectiveness of the antibacterial properties. In this study, hydrogel coating was loaded with clinically used antimicrobial agents including PVP-I, copper ions, and

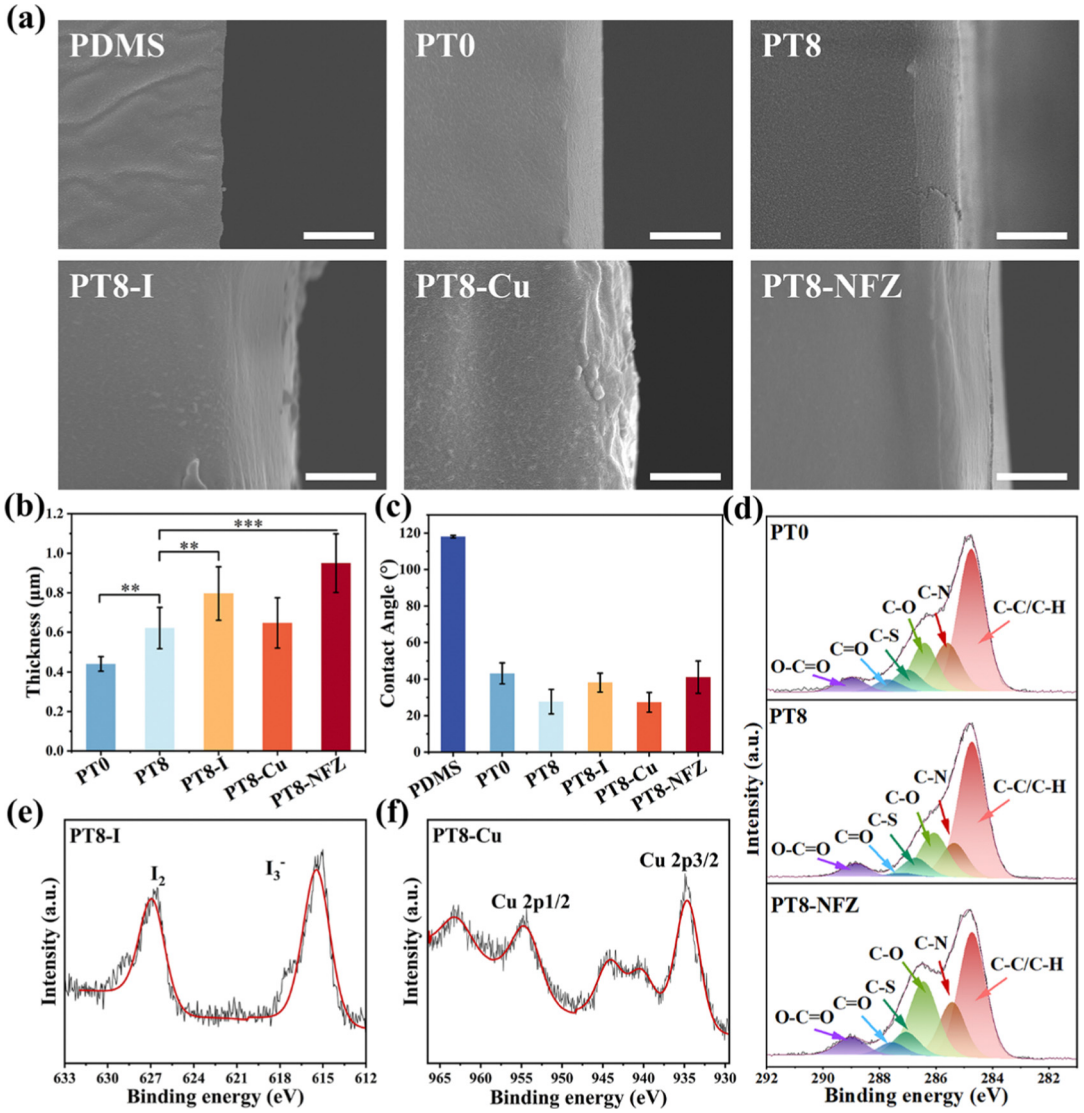

Fig. 1 (a) SEM images of the cross-section of pristine and modified PDMS. Scale bars represent 1 μm. (b) Thickness of hydrogel coating on PDMS. (c) Water contact angles of pristine and modified PDMS surfaces. (d) C 1s, (e) I 3d, and (f) Cu 2p core-level XPS spectra of modified PDMS surfaces.

nitrofurazone *via* various types of non-covalent interactions (Fig. 2a). For instance, PVP-I molecules were loaded in the coating *via* hydrogen bonding and electrostatic interaction with TA molecules and the zwitterionic groups.[27] As a result, the iodine content loaded in the PT8 coating was 5.22 mg cm^{-2}, which was 2.4 times and 6.2 times higher than that of PT0 (2.20 mg cm^{-2}) and PDMS (0.84 mg cm^{-2}). Copper ions could be chelated by the deprotonated phenolic groups of TA,[10] and electrostatically complexed with the anionic group $-SO_3^-$ of polySBMA. The copper content loaded in PT8 coating was 4.44 μg cm^{-2}, which was significantly higher than that of PT0 (0.12 μg cm^{-2}) and PDMS (0.01 μg cm^{-2}). The content of nitrofurazone in PT8 (26.29 μg cm^{-2}) was also much higher than that in PT0 (3.31 μg cm^{-2}) and PDMS (4.59 μg cm^{-2}). This is attributed to the fact that the nitrofurazone molecules were immobilized by the zwitterionic group of polySBMA *via* electrostatic interaction and hydrogen bonding.[28] Based on the various and multiple binding sites for non-covalent interactions provided by the TA molecules and zwitterionic groups, the PT8 hydrogel coating showed a universal loading capability and a high loading efficiency with various types of antimicrobial agents.

3.3 pH-Responsive release of antimicrobial agents

The urine of a healthy adult is slightly acidic or neutral with a pH value of 4.5–7.8.[29] However, if the urinary tract is infected by urease-producing pathogens such as *P. mirabilis*, the pH of the urine would dramatically increase to as high as 9–10 within 1 or 2 days.[18,21,30] Therefore, an effective strategy for the control of CAUTIs and consequent encrustation is the development of a smart antibacterial coating which could sense the urine pH, maintain a low release rate of antimicrobial agents under ordinary conditions, and increase the release rate once an infection with urease-producing bacteria occurs. In this study,

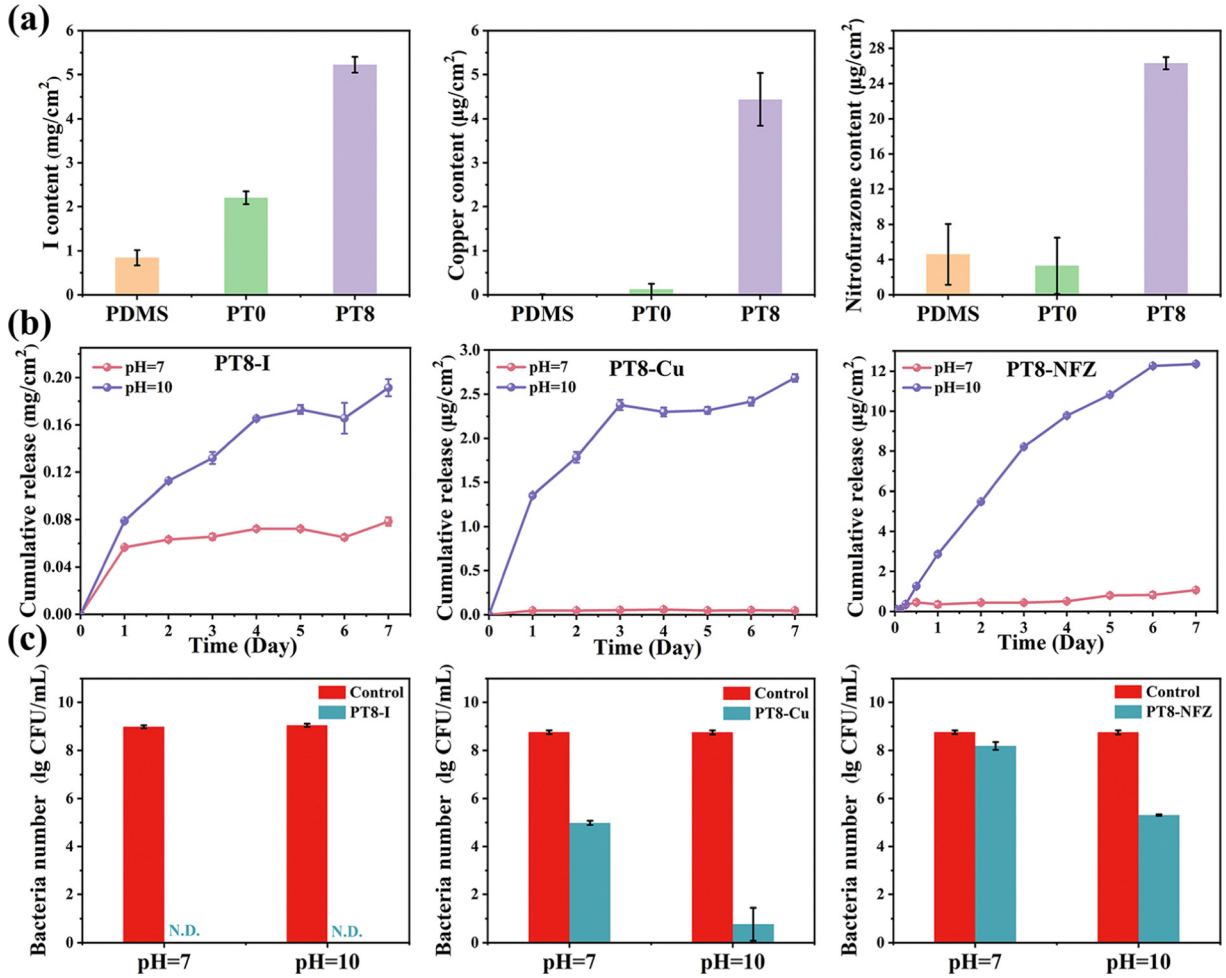

Fig. 2 (a) Contents of iodine, copper, and nitrofurazone on the PDMS surface, and PT0 and PT8 hydrogel coatings. (b) Release of iodine, copper, and nitrofurazone from PT8-I, PT8-Cu and PT8-NFZ, respectively over 7 days in neutral (pH = 7) and alkaline (pH = 10) conditions. (c) Bactericidal property of PT8-I, PT8-Cu and PT8-NFZ against *P. mirabilis* under neutral (pH = 7) and alkaline (pH = 10) conditions.

all the hydrogel coatings loaded with antimicrobial agent exhibited a relatively low release rate under neutral conditions (Fig. 2b). After 7 days of immersion, approximately 0.08 mg cm^{-2} of iodine, 0.05 μg cm^{-2} of copper, and 1.06 μg cm^{-2} of nitrofurazone were released from the coating under neutral conditions (pH = 7). However, when the pH increased to 10, the release amount of iodine, copper, and nitrofurazone significantly increased to 0.19 mg cm^{-2} of iodine, 2.69 μg cm^{-2} of copper, and 12.36 μg cm^{-2} of nitrofurazone (*i.e.* 2.37 times, 53.80 times, and 111.66 times, respectively) over 7 days. The pH-responsive manner of antimicrobials released from the hydrogel coating could be attributed to the non-covalent interactions between the antimicrobial agents and hydrogel coating being disrupted under the alkalized conditions. Under alkalized conditions, iodine in PVP-I was ionized to I^- and IO_3^-, which could be electrostatically repelled by the zwitterionic group of polySBMA.[31] The phenolic hydroxyl groups in TA could be oxidized to quinones, which has a low affinity with copper ions, leading to disintegration of the TA-Cu network.[10] For the PT8-NFZ coating, nitrofurazone could be deprotonated under alkalized conditions. As a result, the hydrogen bonding between nitrofurazone and zwitterionic groups was damaged, and the nitrofurazone molecules adsorbed on the $-SO_3^-$ groups were electrostatically repelled from the polymer chains. In addition, when the pH increases, the hydrogen bonding between TA and polySBMA was destroyed, and it further contributed to the enhanced release of antimicrobial agents.[32] Furthermore, the antibacterial properties of the hydrogel coatings in different pH conditions were evaluated (Fig. 2c). As can be seen, the bactericidal activity of PT8-Cu and PT8-NFZ increased by 4.22 log and 2.87 log when the pH value of the solution increased from 7 to 10, which is consistent with the results that more antimicrobial agents were released from the coating and killed the bacteria. For the PT8-I coating, no viable bacteria were detected in the solution with a pH of 7 and 10. This is probably because the initial release rate of iodine from the coating is high (Fig. 2b, 0.057 mg cm^{-2} and 0.079 mg cm^{-2} in pH of 7 and 10 over 1 day, respectively), so most of the bacteria were killed even under neutral conditions. The loading and release of iodine were much higher than those of Cu^{2+} and

nitrofurazone in the hydrogel coating, resulting in the best antibacterial performance of PT8-I. All three antimicrobial agent-loaded hydrogel coatings have significantly higher antibacterial properties compared to the hydrogel coating without antimicrobial. Nevertheless, the PT8 hydrogel coating had a high loading efficiency for various antimicrobial agents, and the release behavior of the antimicrobial agents showed a pH-responsive manner, and enhanced its bactericidal property under alkalized conditions. The hydrogel coating with high antimicrobial agent loading efficiency and pH-responsive manner has great potential for antibacterial urinary catheter applications.

3.4 Antibacterial properties of hydrogel coating

Bacterial cells initially adhere on the catheter surface, followed by colonization and biofilm formation, which subsequently resulted in catheter infection. Therefore, inhibition of the initial bacterial adhesion and consequent biofilm formation is crucial for the control of CAUTIs. In this study, two pathogenic bacteria associated with UTIs, namely, *E. coli* and *P. mirabilis* were selected. Adhesion of *E. coli* on the surface of pristine and modified PDMS was first investigated. A large number of adherent bacteria were observed on the pristine PDMS, and the PT0-coated surface showed a certain inhibitory effect (Fig. 3a). The water contact angle of PT0 was greatly reduced (Fig. 1c), indicating that the polySBMA hydrogel layer has a high hydration capacity, which formed a tightly bound water layer on the surface through electrostatically induced hydration, and could contribute to the inhibitory effect of bacterial adhesion.[33] Decreased bacterial adhesion on the hydrogel coating with TA (PT8) was observed. TA has been reported to show antibacterial properties,[34] and thus killed bacterial cells approaching the surface. Loading of antimicrobial agents in the coating further decreased the number of adherent bacteria. Colonies cultured after sliding the substrate onto an agar plate also showed a similar inhibitory effect on bacterial adhesion on the various surfaces (Fig. S3, ESI†). Quantitative analysis confirmed that the hydrogel coating

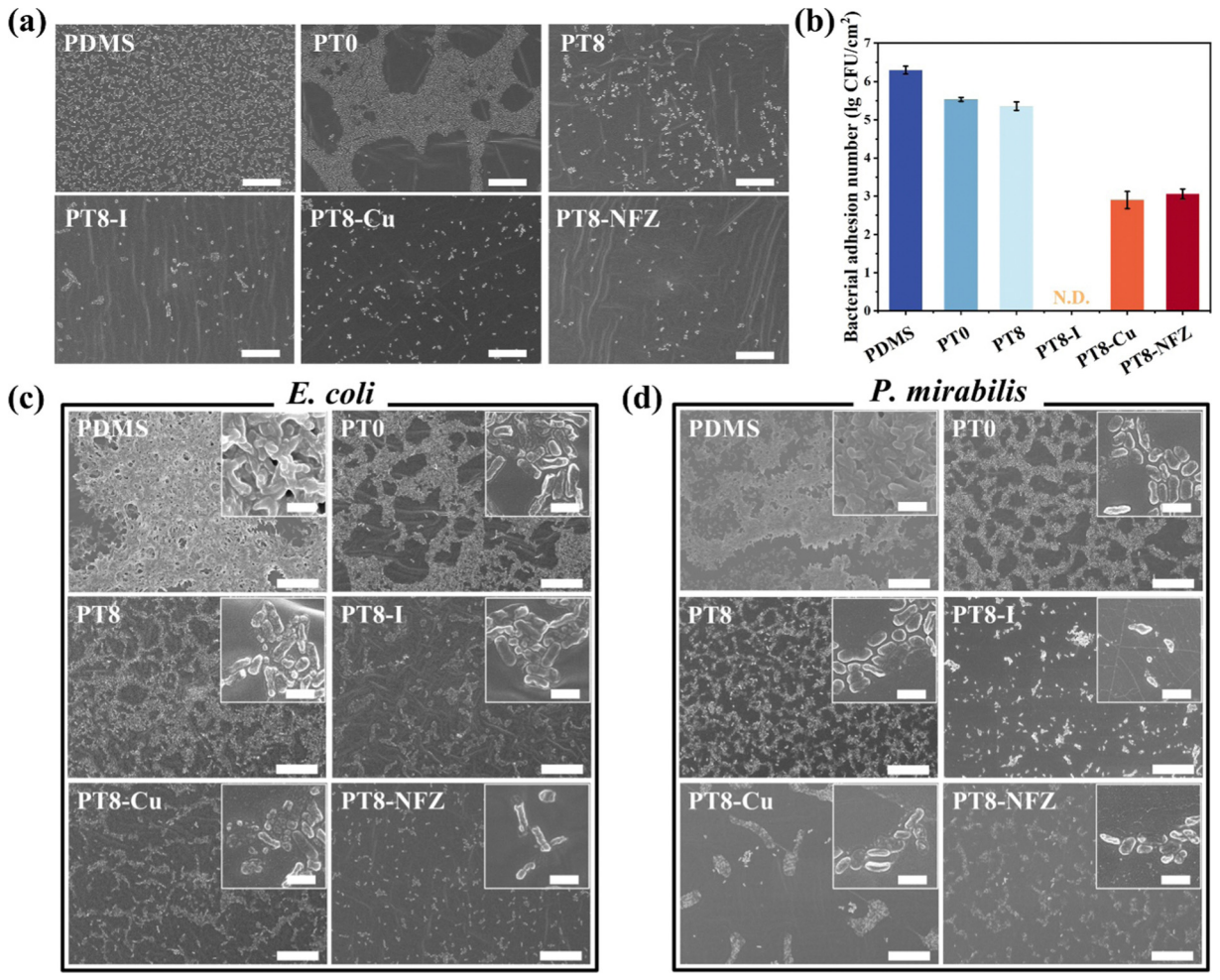

Fig. 3 (a) *E. coli* adhesion on pristine and modified PDMS surfaces after exposure to PBS bacterial suspension (10^8 CFU per mL) for 4 h. Scale bars represent 20 μm. (b) Number of *E. coli* cells adhering on pristine and modified PDMS surfaces. Biofilm formation on pristine and modified PDMS surfaces after 72 h incubation in growth medium containing 10^5 CFU per mL of (c) *E. coli*, and (d) *P. mirabilis* for 72 h. Scale bars in (c) and (d) represent 20 μm and 2 μm in the main images and insets, respectively.

reduced the bacterial number on the surface, and loading of Cu and nitrofurazone reduced the adherent bacterial number by 3.40 and 3.24 orders of magnitude (Fig. 3b). Interestingly, no viable bacteria were harvested from the coating with PVP-I, indicating the excellent bactericidal efficacy of the PT8-I coating, and the results are consistent with the high release rate of iodine from the coating (Fig. 2b).

Biofilm formation on pristine and hydrogel-coated surfaces over a prolonged period was also investigated. As can be seen, *E. coli* and *P. mirabilis* colonized heavily on the pristine PDMS surface over 24 h (Fig. S4 and S5, ESI†), while the PT0 coating reduced the number of colonized bacteria, but most of the bacterial cells were viable, which was because the PT0 coating resisted bacterial adhesion but had a lack of bactericidal activity. The PT8 coating further inhibited bacterial colonization, and with the loading of antimicrobial agents, the surface showed few bacterial cells, and the cell membrane of the existing bacteria was damaged. Further incubation of the substrates over 72 h confirmed the pronounced antibacterial properties of the antimicrobial-loaded hydrogel coatings (Fig. 3c and d). Since long-term catheterization usually requires the catheter to be in place for more than 7 days, the period of biofilm culture was extended to 10 days in this study. As can be seen from the qualitative results (Fig. S6 and S7, ESI†) and quantitative results (Fig. S8, ESI†), all of the three hydrogel coatings with antimicrobials showed antibacterial properties up to 7 days with very few bacterial cells found on the slid agar plates (Fig. S6, ESI†) and the substrate surfaces (Fig. S7, ESI†). The bacterial continued to grow at Day 10, and the PT8-I still showed a pronounced antibacterial capability against both *E. coli* and *P. mirabilis*. The quantitative results showed that the number of bacterial cells on the PT8-I surface was reduced by >3.87 orders of magnitude compared to the pristine PDMS surface on day 7 (Fig. S8, ESI†). The bacteria continued to proliferate even on the antimicrobial-loaded hydrogel surface, but >2.01 orders of magnitude of bacterial reduction were achieved on day 10 compared to the pristine PDMS surface. Both the anti-adhesive properties of the hydrogel layer and the bactericidal activity of TA and antimicrobial agents contributed to the excellent antimicrobial performance of the coatings, and thus prevented the surface from bacterial contamination.

3.5 Coating stability assay

Urinary catheters would be subjected to frictional forces during insertion in the urethra. Therefore, the antibacterial properties and surface hydrophilicity of the hydrogel coating on a PDMS ball after friction movement over a distance of 300 cm ($\sim$10 times the length of a urinary catheter) were explored to evaluate the stability of the hydrogel coatings. As can be seen in Fig. S9 (ESI†), the PT8 surface maintained an obvious inhibitory effect on bacterial adhesion. On the surface of antimicrobial-loaded hydrogel coatings (PT8-I, PT8-Cu, and PT8-NFZ), very few bacteria were found (Fig. S9b, ESI†), which was similar to that of the antimicrobial-loaded hydrogel coatings before the friction test (Fig. S9a, ESI†). SEM images also confirmed the coatings after friction could effectively inhibit bacterial adhesion on the surfaces (Fig. S9c, ESI†). The water contact angles of the surfaces before and after the friction test were comparable, with no significant difference observed (Fig. S9d, ESI,† compared to Fig. 1c).

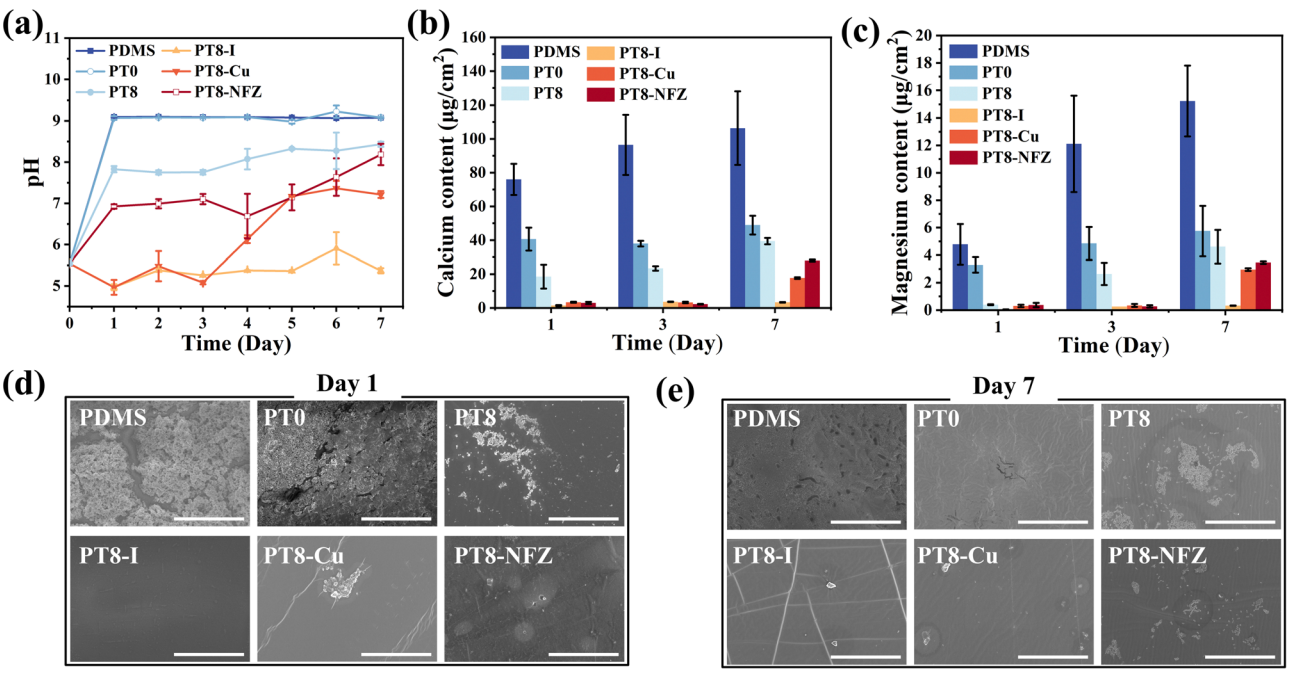

Fig. 4 (a) Change in pH value of artificial urine inoculated with 10^5 CFU per mL of *P. mirabilis* containing pristine and modified PDMS substrate over 7 days. The content of (b) calcium and (c) magnesium elements deposited on the surface of pristine and modified PDMS after incubating in artificial urine containing *P. mirabilis* over 7 days. SEM images of pristine and modified PDMS surfaces after an encrustation test for (d) 1 day and (e) 7 days. Scale bars represent 50 μm.

These results confirmed that the hydrogel coatings were stable under the frictional forces, which was a key characteristic for their use in urinary catheter applications.

3.6 *In vitro* encrustation assay

A significant challenge in urinary catheter application is the formation of encrustation on the catheter surface, and

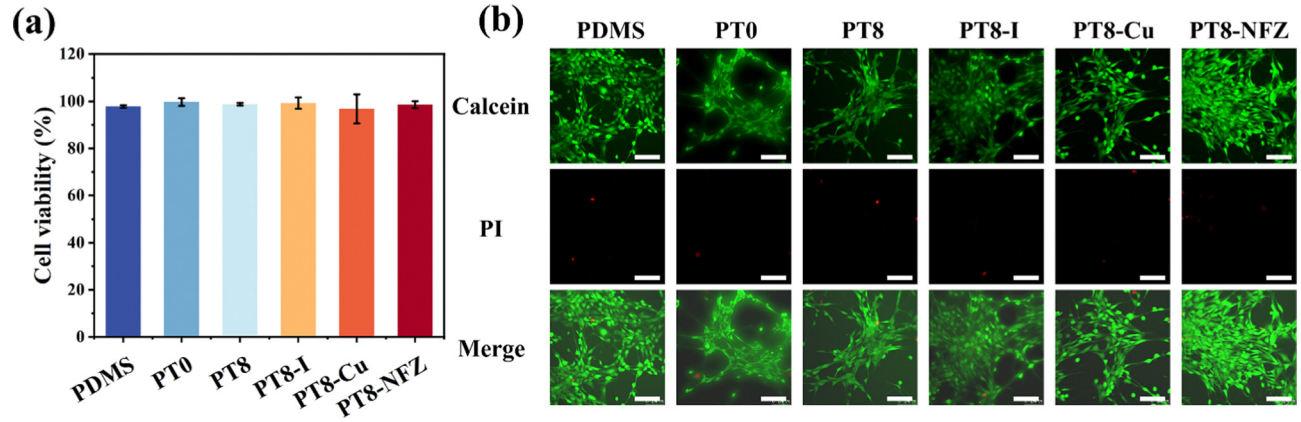

Fig. 5 (a) Cell viability of NIH/3T3 fibroblasts after incubation in extract medium of pristine and modified PDMS for 24 h. (b) CLSM images of NIH/3T3 fibroblast cells incubated in extract medium of pristine and modified PDMS for 24 h. Scale bars represent 100 μm.

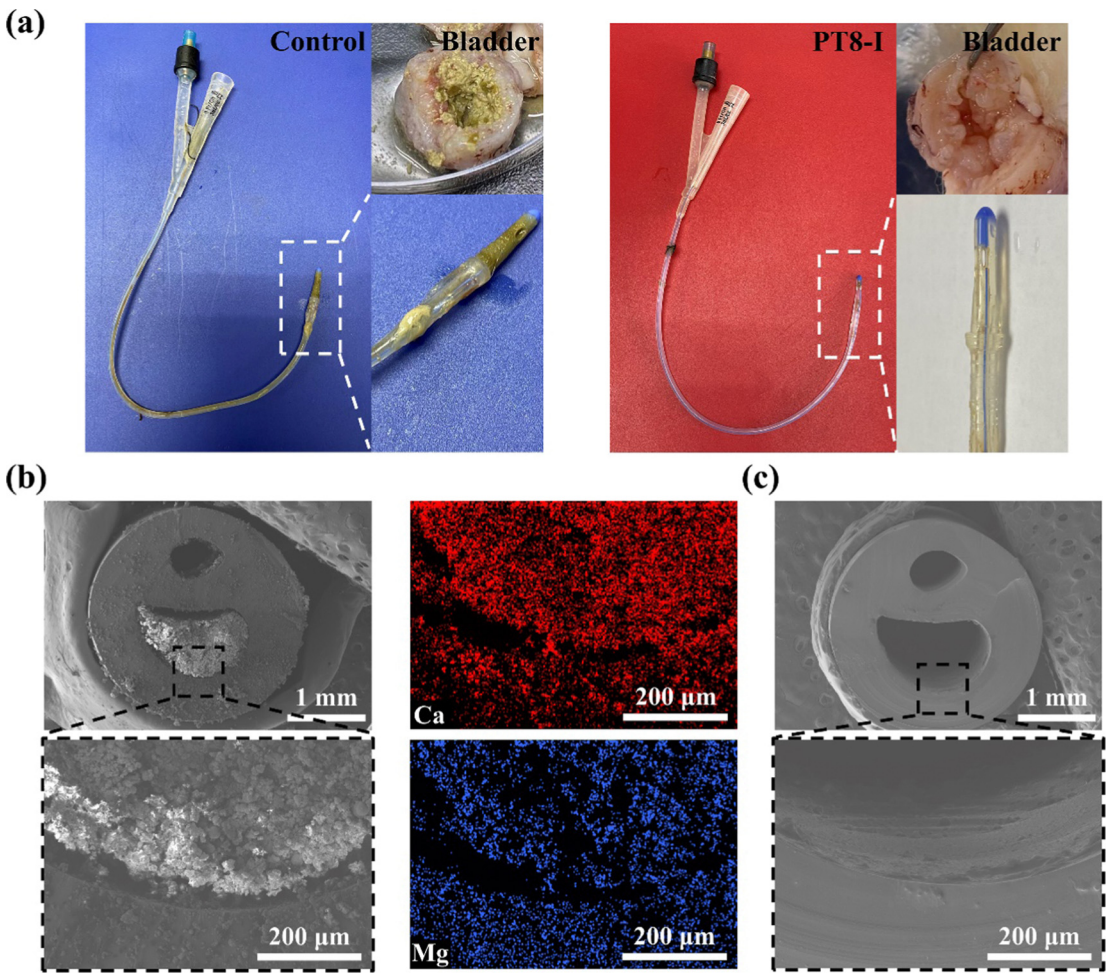

Fig. 6 (a) Photographs of a catheter and rabbit bladder harvested from an animal after implantation for 7 days. (b) SEM images and EDS mapping of cross-section of unmodified catheter after implantation for 7 days. (c) SEM images of cross-section of PT8-I-coated catheter after implantation for 7 days.

subsequent blockage of the catheter lumen.[3] As mentioned, urease-producing pathogen like *P. mirabilis* generates urease, which decomposes urea into ammonia and increases the urine pH. Calcium and magnesium ions deposit in the alkalized urine in the forms of calcium phosphate and magnesium phosphate, accumulate and form encrustation in the catheter lumen, increasing the risk of upstream infection and even death. In this study, the capability of the hydrogel coating in inhibiting bacteria-induced encrustation formation was investigated by incubating the substrates in *P. mirabilis*-inoculated artificial urine. The bacteria-containing artificial urine was changed daily over 7 consecutive days, to mimic a continuous infection situation in the urinary catheter. The pH value of the artificial urine was recorded every day, and encrustation formation on the substrate surface was monitored. As can be seen, the pH of the urine with pristine and PT0-coated PDMS rose to above 9 on the first day, and remained around 9 thereafter (Fig. 4a). PT8 coating slightly inhibited the increase of urine pH, probably due to the bactericidal capability and acidic nature of TA. With the antimicrobial agent-loaded hydrogel coating, the pH of the urine was maintained below 7 for at least 4 days, due to the released antimicrobial agents effectively killing the *P. mirabilis* cells, and inhibited the process of alkalization of the urine. Interestingly, with the PT8-I coating, the urine stayed acidic over 7 days, confirming the strong bactericidal property of the PT8-I coating. The contents of calcium and magnesium elements on the surface of each substrate were measured using ICP-OES (Fig. 4b and c). The contents of calcium and magnesium on the pristine PDMS surface were high, and increased over 7 days, and thick films comprising bacterial cells and crystals were observed on the pristine PDMS surface (Fig. 4d and e). Salt deposition on the PT0 and PT8 coating was inhibited, but there were still a high amount of Ca and Mg salts on the surface. The antimicrobial agent-loaded hydrogel coating effectively inhibited encrustation formation, and in the first 3 days, the surface stayed relatively clean with few salt deposits. It is worth mentioning that the PT8-I surface maintained free of encrustation for up to 7 days. These results indicated that the antimicrobial agent-loaded hydrogel coating had good bactericidal performance

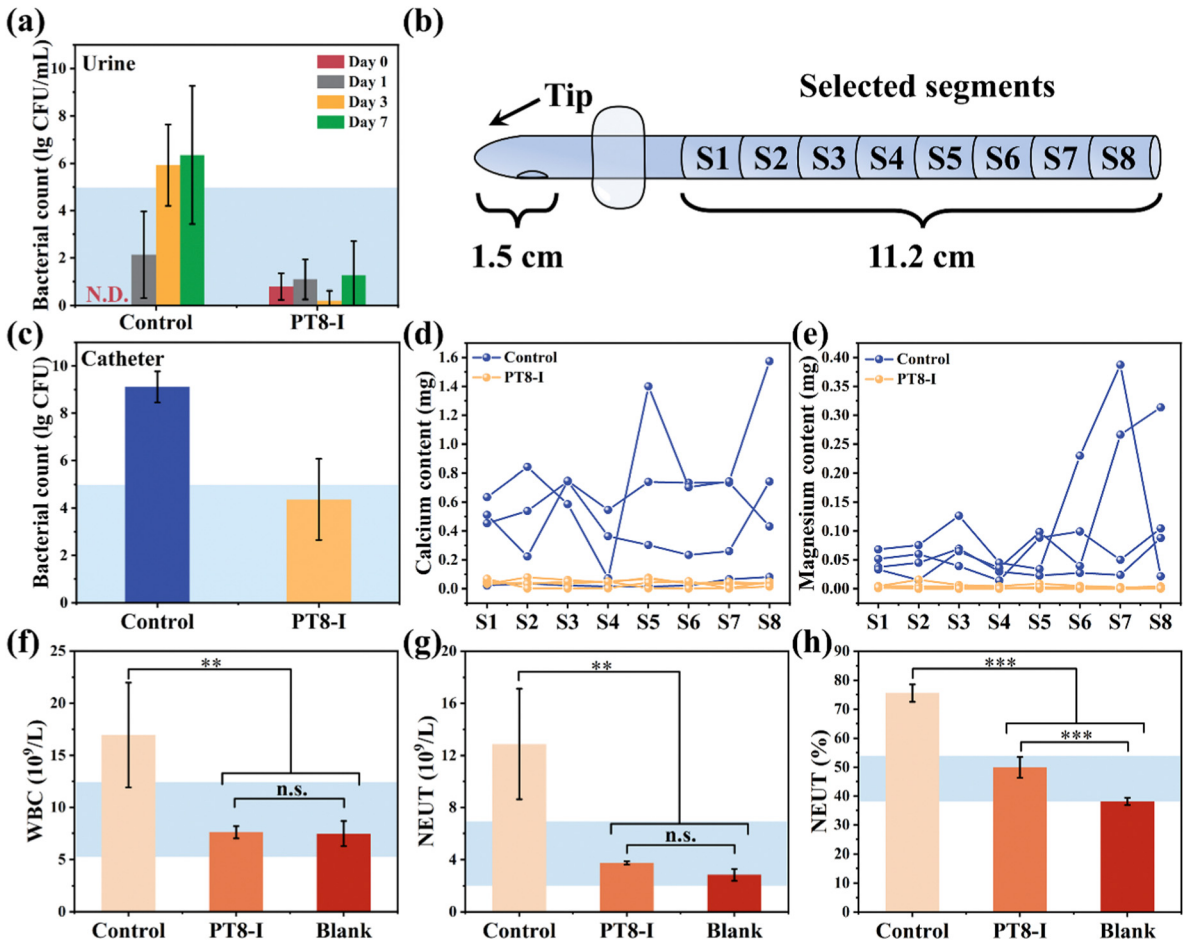

Fig. 7 (a) Count of bacteria in the urine over 7 days of catheter implantation in rabbits. (b) Schematic representation of sections of the catheter used for determination of the bacterial number and encrustation formation. (c) Number of bacteria colonized on the catheter tip (1.5 cm in length) after catheter insertion in rabbits for 7 days. The contents of (d) calcium and (e) magnesium on the segment of the catheter after implantation for 7 days. (f) White blood cell count, (g) total neutrophil count, and (h) neutrophil ratio of the blood collected from the animals after implantation for 7 days (n = 4). The blue area represents the normal reference range.

against urease-producing *P. mirabilis*, and inhibited encrustation formation, and the PT8-I coating showed the best effect.

3.7 *In vitro* cytotoxicity

Any potential cytotoxic substance from the coating was extracted, and the cytotoxicity was evaluated using a CCK-8 assay and live/dead staining with 3T3 fibroblasts. The cell viability of all groups with pristine PDMS, and PDMS with hydrogel coating and antimicrobial agent was >96.8% (Fig. 5). Furthermore, the cells cultured with the extract of pristine and modified PDMS substrates were almost green after staining, with few dead cells observed. The results showed that the antimicrobial agent-loaded hydrogel coating on PDMS had good biocompatibility and negligible cytotoxicity.

3.8 *In vivo* implantation study

The ultimate goal of the hydrogel-coated catheter is for implantation in the body. Therefore, the *in vivo* performance of the coating should be evaluated before moving forward for clinical application. The *in vitro* results above showed PT8-I coating has the best antibacterial and anti-encrustation formation properties, and good biocompatibility. In the following study, full-size urinary catheters with PT8-I coating were prepared and implanted in rabbits. After implantation for 7 days, the catheter was removed from the rabbit for evaluation. Large amounts of metabolites and crystals were deposited on the catheter tip in the control group (Fig. 6a). The catheter lumen was completely blocked, and there were a large number of crystals and bacterial deposits in the bladder. In contrast, the PT8-I-coated catheter was relatively clean, without blockage observed. No obvious encrustation was found in the bladder. SEM images showed that the catheter lumen in the control group was filled with encrustation crystals (Fig. 6b), which contained a large amount of calcium and magnesium (Fig. S10, ESI†). In contrast, the lumen of the PT8-I-coated catheter was clean and remained free of encrustation (Fig. 6c), indicating that the PT8-I coating was effective in inhibiting bacterial infection and encrustation formation *in vivo*.

It should be noted that in the animal study, no urine collection bag was used, and the catheter remained open throughout the experiment. Therefore, microorganisms from the external environment could migrate through the catheter lumen spontaneously, and cause infection in the animal. The bacterial number in the urine was recorded (Fig. 7a). The initial number of bacteria in the urine was negligible. However, after 3 days, the bacterial number increased to $>10^5$ CFU per mL in the control group, indicating bacteriuria occurred in the animal.[35] For the PT8-I group, the bacterial number in the urine remained below 10^2 CFU per mL over 7 days, showing that the coating could prevent bacteria growth in the urine. The harvested catheter was sectionized for bacterial counting and encrustation quantification (Fig. 7b). The bacterial count on the surface of the control catheter tip (1.5 cm in length) was 1.3×10^9 CFU (Fig. 7c), indicating that the catheter was heavily colonized by bacteria. In contrast, the bacterial number on the PT8-I-coated catheter tip was 2.3×10^4 CFU. These results indicated that PT8-I-coated catheters could significantly reduce bacterial colonization. The calcium and magnesium deposited on different positions of the catheter were quantified by ICP-OES. As can be seen, encrustation formation on the surface of the PT8-I coating was significantly inhibited along the catheter, compared to that of the control group (Fig. 7d and e). This is consistent with the results of the *in vitro* encrustation experiment, which showed that the PT8-I coating had an excellent anti-encrustation capability due to its strong antibacterial properties and release of antibacterial agents. The blood test results showed that the typical immune-related indicators including white blood cell count (WBC), neutrophil count (NEUT), and neutrophil ratio (NEUT%)[36] of the animals of the PT8-I group were in the normal range (Fig. 7f–h),[37] while those of the control group were significantly higher than the reference values, indicating bacterial infection occurred in the animal.

The bladder, urethra, and kidney of the rabbit were collected after 7 days of implantation for histological analysis. H & E staining images showed that significant neutrophils infiltrated the bladder tissue of the control group, indicating inflammation in the bladder tissue (Fig. 8a), while it was significantly reduced in the PT8-I group. Significant neutrophil infiltration and a high number of vacuoles were observed in the inner urethra of the control group (Fig. 8b). In contrast, fewer vacuoles but more normal epithelial cells were found in the PT8-I group. No obvious inflammatory response was observed in the kidney tissue in all the animals (Fig. S11, ESI†). It is suggested that the PT8-I coating on the urinary catheter reduced bacteria invasion into the bladder tissue, and thus,

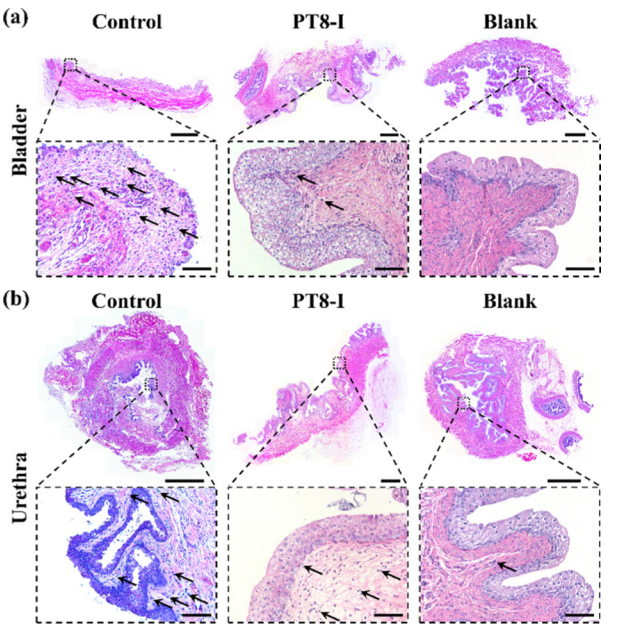

Fig. 8 Representative images of H & E stained (a) bladder, and (b) urethra of rabbit of the control group, PT8-I group, and blank group (without catheterization) after 7 days of study. Scale bars in the main images and insets represent 2 mm and 100 μm, respectively. The black arrows indicate inflammatory cells.

inhibited bacterial colonization and encrustation formation, and maintained a clean urinary tract system.

4. Conclusions

In summary, a pH-responsive hydrogel coating with antibacterial and anti-encrustation formation properties was developed in this study. The polySBMA-TA hydrogel coating showed high loading efficiency with various types of antimicrobial agents, attributed to the multiple non-covalent interactions between the hydrogel coating and the antimicrobials. The non-covalent interactions between antimicrobials and hydrogel coating could be disrupted subjected to the alkalization of the urine, resulting in pH-responsive release of antimicrobials to inhibit infection and bacteria-inducing encrustation. Both *in vitro* and *in vivo* studies confirmed that the coatings have excellent antibacterial, anti-encrustation formation properties, and good biocompatibility. Although there are positive results from this study, it should be noted that there are still some challenges before the hydrogel-coated catheters can be moved into clinical practices. For example, more species and even a mixture of different uropathogens should be used to verify the antibacterial and anti-encrustation properties of the coatings in a more mimicking condition. In addition, studies with prolonged catheterization in big animal models need to be performed. Nevertheless, this antibacterial hydrogel coating with a convenient and efficient antimicrobial-impregnation procedure, enhanced antibacterial properties, and an excellent pH-responsive release profile provides clinical practitioners with great convenience for the control of urinary catheter infections and encrustations, and thus holds great promise in urinary catheter applications.

Author contributions

Jiru Miao: conceptualization, methodology, formal analysis, investigation, data curation, and writing – original draft; Xiang Wu: methodology, investigation, and resources; Yue Fang: investigation and resources; Mingzhu Zeng: investigation; Zhimao Huang: investigation; Mi Ouyang: investigation, resources, supervision, and funding acquisition; Rong Wang: conceptualization, methodology, resources, writing – review & editing, supervision, project administration, and funding acquisition.

Conflicts of interest

There are no conflicts of interest to declare.

Acknowledgements

This work was supported by the National Key Research and Development Program of China (2018YFE0119400), the National Natural Science Foundation of China (51803229, 52011530019, 52073257), the Youth Innovation Promotion Association CAS (2021296), and the Key Research and Development Program of Ningbo (2022Z132).

References

1 S. S. Magill, J. R. Edwards, W. Bamberg, Z. G. Beldavs, G. Dumyati, M. A. Kainer, R. Lynfield, M. Maloney, L. McAllister-Hollod, J. Nadle, S. M. Ray, D. L. Thompson, L. E. Wilson and S. K. Fridkin, *N. Engl. J. Med.*, 2014, **370**, 1198–1208.
2 P. Singha, J. Locklin and H. Handa, *Acta Biomater.*, 2017, **50**, 20–40.
3 D. J. Stickler and R. C. L. Feneley, *Spinal Cord*, 2010, **48**, 784–790.
4 Q. Yao, C. S. Wu, X. Y. Yu, X. Chen, G. Q. Pan and B. H. Chen, *Mater. Today Bio.*, 2022, **16**, 100413.
5 S. I. C. Ricardo, I. I. L. Anjos, N. Monge, C. M. C. Faustino and I. A. C. Ribeiro, *ACS Infect. Dis.*, 2020, **6**, 3109–3130.
6 E. M. J. Lin, C. L. Lay, G. S. Subramanian, W. S. Tan, S. S. J. Leong, L. C. H. Moh and K. Lim, *ACS Appl. Mater. Interfaces*, 2021, **13**, 59263–59274.
7 Q. Yao, J. Zhang, G. Pan and B. Chen, *ACS Appl. Mater. Interfaces*, 2022, **14**, 36473–36486.
8 Q. Yao, B. H. Chen, J. X. Bai, W. B. He, X. Chen, D. C. Geng and G. Q. Pan, *J. Mater. Chem. B*, 2022, **10**, 2584–2596.
9 R. Wang, K. G. Neoh, E. T. Kang, P. A. Tambyah and E. Chiong, *J. Biomed. Mater. Res. Part B Appl. Biomater.*, 2015, **103**, 519–528.
10 Z. M. Huang, D. W. Zhang, Q. W. Gu, J. R. Miao, X. Cen, R. P. Golodok, V. V. Savich, A. P. Ilyushchenko, Z. S. Zhou and R. Wang, *RSC Adv.*, 2022, **12**, 15685–15693.
11 M. Douglass, S. Ghalei, E. Brisbois and H. Handa, *ACS Appl. Bio Mater.*, 2022, **5**, 700–710.
12 K. Belfield, X. Y. Chen, E. F. Smith, W. Ashraf and R. Bayston, *Acta Biomater.*, 2019, **90**, 157–168.
13 J. N. Lee, C. Park and G. M. Whitesides, *Anal. Chem.*, 2003, **75**, 6544–6554.
14 S. Perni, C. Piccirillo, J. Pratten, P. Prokopovich, W. Chrzanowski, I. P. Parkin and M. Wilson, *Biomaterials*, 2009, **30**, 89–93.
15 C. Traba and J. F. Liang, *J. Controlled Release*, 2015, **198**, 18–25.
16 S. M. Jacobsen, D. J. Stickler, H. L. T. Mobley and M. E. Shirtliff, *Clin. Microbiol. Rev.*, 2008, **21**, 26–59.
17 D. J. Stickler, S. M. Jones, G. O. Adusei and M. G. Waters, *J. Clin. Microbiol.*, 2006, **44**, 1540–1542.
18 S. Malic, M. G. J. Waters, L. Basil, D. J. Stickler and D. W. Williams, *J. Biomed. Mater. Res. Part B Appl. Biomater.*, 2012, **100**, 133–137.
19 S. Milo, F. B. Acosta, H. J. Hathaway, L. A. Wallace, N. T. Thet and A. T. A. Jenkins, *ACS Sens.*, 2018, **3**, 612–617.
20 S. Milo, H. Hathaway, J. Nzakizwanayo, D. R. Alves, P. P. Esteban, B. V. Jones and A. T. A. Jenkins, *J. Mater. Chem. B*, 2017, **5**, 5403–5411.
21 J. Zhou, S. Hou, L. H. Li, D. Y. Yao, Y. Y. Liu, A. T. A. Jenkins and Y. B. Fan, *Adv. Mater. Interfaces*, 2018, **5**, 1801242.
22 Y. Yu, H. Yuk, G. A. Parada, Y. Wu, X. Y. Liu, C. S. Nabzdyk, K. Youcef-Toumi, J. F. Zang and X. H. Zhao, *Adv. Mater.*, 2019, **31**, 1807101.

23 K. Fang, Q. W. Gu, M. Z. Zeng, Z. M. Huang, H. F. Qiu, J. R. Miao, Y. Fang, Y. Y. Zhao, Y. Xiao, T. Xu, R. P. Golodok, V. V. Savich, A. P. Ilyushchenko, F. R. Ai, D. L. Liu and R. Wang, *J. Mater. Chem. B*, 2022, **10**, 4142–4152.
24 K. Yu, A. Alzahrani, S. Khoddami, J. T. J. Cheng, Y. Mei, A. Gill, H. D. Luo, E. F. Haney, K. Hilpert, R. E. W. Hancock, D. Lange and J. N. Kizhakkedathu, *ACS Appl. Mater. Interfaces*, 2021, **13**, 36784–36799.
25 R. A. MacPhee, J. Koepsel, T. Tailly, S. K. Vangala, L. Brennan, P. A. Cadieux, J. P. Burton, C. Wattengel, H. Razvi and J. Dalsin, *J. Endourol.*, 2019, **33**, 590–597.
26 H. Phuengkham and N. Nasongkla, *J. Mater. Sci.: Mater. Med.*, 2015, **26**, 78.
27 J. L. Ma, Y. Zhang, D. Q. Zhang, X. J. Niu and Z. Lin, *Chem. Eng. J.*, 2022, **430**, 132276.
28 F. Y. Deng, C. Y. Dong and Y. Liu, *Mol. BioSyst.*, 2012, **8**, 1446–1451.
29 M. R. Clarkson, C. N. Magee and B. M. Brenner, in *Pocket Companion to Brenner and Rector's The Kidney*, ed. M. R. Clarkson, C. N. Magee, B. M. Brenner, W. B. Saunders, New York, 8th edn, 2011, vol. 2, pp. 21–41.
30 L. Wang, S. Zhang, R. Keatch, G. Corner, G. Nabi, S. Murdoch, F. Davidson and Q. Zhao, *J. Hosp. Infect.*, 2019, **103**, 55–63.
31 A. Sa, S. Sawatdee, N. Phadoongsombut, W. Buatong, T. Nakpeng, R. Sritharadol and T. Srichana, *Acta Pharm.*, 2017, **67**, 169–186.
32 T. Shutava, M. Prouty, D. Kommireddy and Y. Lvov, *Macromolecules*, 2015, **38**, 2850–2858.
33 Z. Q. Zhu, Q. Gao, Z. Y. Long, Q. Y. Huo, Y. F. Ge, N. Vianney, N. A. Daliko, Y. C. Meng, J. Qu, H. Chen and B. L. Wang, *Bioact. Mater.*, 2021, **6**, 2546–2556.
34 Y. X. Yang, X. D. Zhao, J. Yu, X. X. Chen, R. Y. Wang, M. Y. Zhang, Q. Zhang, Y. F. Zhang, S. Wang and Y. L. Cheng, *Bioact. Mater.*, 2021, **6**, 3962–3975.
35 V. L. Tchesnokova, E. Rechkina, D. Chan, H. G. Haile, L. Larson, K. Ferrier, D. W. Schroeder, T. Solyanik, S. Shibuya, K. Hansen, J. D. Ralston, K. Riddell, D. Scholes and E. V. Sokurenko, *Clin. Infect. Dis.*, 2020, **70**, 937–939.
36 B. H. Foy, T. M. Sundt, J. C. T. Carlson, A. D. Aguirre and J. M. Higgins, *Nat. Commun.*, 2022, **13**, 4705.
37 D. M. Moore, K. Zimmerman and S. A. Smith, *Vet. Clin. North Am.*, 2015, **18**, 9–19.

